The official journal of
INTERNATIONAL FEDERATION OF PIGMENT CELL SOCIETIES · SOCIETY FOR MELANOMA RESEARCH

PIGMENT CELL & MELANOMA Research

Copy Number Analysis in Congenital Nevi: Concordance and Diagnostic Limitations of aCGH, sWGS, and Methylation Sequencing

Anton Karelin[1] | Ines B. Brecht[2] | Michaela Pogoda[1,3] | German Demidov[1] | Michael Abele[2] | Dominik T. Schneider[4] | Daniel Aldea[5] | Heather C. Etchevers[5] | Susana Puig[6,7] | Matthias Hahn[8] | Christopher Schroeder[1] | Stephan Forchhammer[8] | on behalf of the MELCAYA consortium

DOI: 10.1111/pcmr.70097

Pigment Cell & Melanoma Research

WILEY

ORIGINAL ARTICLE OPEN ACCESS

Copy Number Analysis in Congenital Nevi: Concordance and Diagnostic Limitations of aCGH, sWGS, and Methylation Sequencing

Anton Karelin[1] | Ines B. Brecht[2] | Michaela Pogoda[1,3] | German Demidov[1] | Michael Abele[2] | Dominik T. Schneider[4] | Daniel Aldea[5] | Heather C. Etchevers[5] | Susana Puig[6,7] | Matthias Hahn[8] | Christopher Schroeder[1] | Stephan Forchhammer[8] | on behalf of the MELCAYA consortium

[1]Institute of Medical Genetics and Applied Genomics, Eberhard Karls University of Tübingen, Tübingen, Germany | [2]Pediatric Hematology and Oncology, Children's Hospital, Eberhard Karls University of Tübingen, Tübingen, Germany | [3]NGS Competence Center, Tübingen, Germany | [4]Clinic of Pediatrics, Klinikum Dortmund, University Witten/Herdecke, Dortmund, Germany | [5]Aix Marseille University, INSERM, Marseille Medical Genetics, Marseille, France | [6]Dermatology Department, Hospital Clínic de Barcelona, Universitat de Barcelona, Institut de Investigacions Biomediques August Pi I Sunyer (IDIBAPS), Barcelona, Spain | [7]Centro de Investigación BIomédica en Red de Enfermedades Raras (CIBERER), Instituto de Salud Carlos III, Barcelona, Spain | [8]Department of Dermatology, Eberhard Karls University of Tübingen, Tübingen, Germany

Correspondence: Stephan Forchhammer (stephan.forchhammer@med.uni-tuebingen.de)

Received: 4 March 2026 | **Revised:** 18 May 2026 | **Accepted:** 26 May 2026

Keywords: CGH | congenital melanocytic nevus | copy number alteration | DNA methylation sequencing | pediatric melanoma | proliferative nodule | shallow whole-genome sequencing

ABSTRACT

Distinguishing benign proliferative nodules (PNs) from melanoma arising within congenital melanocytic nevi remains a major diagnostic challenge. Copy number alteration (CNA) analysis is widely used to support classification, but current criteria were developed using array comparative genomic hybridization (aCGH). The performance of alternative platforms such as shallow whole-genome sequencing (sWGS) and methylation sequencing is poorly defined in this context. The objective of this study is to compare CNA profiles obtained from aCGH, sWGS, and methylation sequencing in atypical nodules arising within congenital nevi, and to explore their clinical context based on available follow-up data. Sixteen samples from 14 patients were retrospectively analyzed using all three platforms. CNAs were cataloged, concordance across methods was quantified using the Jaccard index, and molecular classifications were compared. Clinical follow-up was reviewed to provide clinical context. aCGH detected 39 CNAs, sWGS 60, and methylation sequencing 66. Concordance was highest between sWGS and methylation (mean Jaccard 0.67), followed by aCGH versus sWGS (0.64) and aCGH versus methylation (0.49). Cases with high aneuploidy demonstrated strong cross-platform agreement, whereas low-burden lesions exhibited greater variability between methods. Divergent molecular classifications were observed in six cases. While all methods reliably detect broad chromosomal changes, sWGS and methylation sequencing identify many additional focal CNAs that may not align with CGH-based diagnostic criteria. These findings highlight the need for platform-adapted thresholds and validation in larger outcome-linked cohorts.

See Supporting Information S1 for the full list of collaborators.

Key Points

- aCGH, sWGS, and methylation sequencing show high concordance for broad chromosomal copy number alterations in atypical nodules arising in congenital nevi.
- Higher-resolution methods detect additional focal CNAs that may alter molecular classification when CGH-derived criteria are applied.
- Platform-specific thresholds and validation in larger outcome-linked cohorts are needed before higher-resolution approaches can be interpreted equivalently to CGH.

1 | Introduction

Pediatric melanoma is a rare neoplasm, with an estimated incidence of four cases per million children and adolescents under 20 years of age annually (Ferrari et al. 2019; Merkel et al. 2019). Incidence rises markedly during puberty and adolescence, where melanoma accounts for approximately 7% of all malignancies among individuals aged 15–19 years (McMullan and Grant-Kels 2025). Most cases occur in adolescents, whereas melanoma in children under 10 years remains exceptionally uncommon (Merkel et al. 2019; Yousif et al. 2021).

Pediatric melanomas comprise several biologically distinct subtypes, including Spitz melanomas, conventional melanomas, melanomas arising within large or giant congenital melanocytic nevi (CMN), and rare variants. Prognosis varies widely between these subgroups. Spitz melanocytomas and Spitz melanomas show a high rate of nodal involvement but low melanoma-specific mortality (Hawryluk et al. 2020; Pampena et al. 2023; Pappo et al. 2021). In contrast, conventional melanomas and melanomas arising in congenital nevi behave more aggressively. Although rare, melanomas arising in CMN account for a disproportionate number of fatal pediatric melanoma cases, particularly in children under five years of age (Hawryluk et al. 2020; Merkel et al. 2019; Pappo et al. 2021).

Diagnosis of melanoma arising in CMN remains challenging. Giant CMN may contain multiple, sometimes rapidly enlarging nodules, and distinguishing benign proliferative nodules (PN) from melanoma can be difficult based on clinical and histologic criteria alone. Histopathologic assessment typically evaluates mitotic activity, ulceration, cytologic atypia, and architectural features to differentiate PNs from melanoma (Merkel et al. 2019; Pavlova et al. 2016; Phadke et al. 2011; Vergier et al. 2016).

Molecularly, PNs and melanomas differ mainly in their patterns of copy number alterations (CNAs). Benign PNs typically exhibit whole-chromosome gains or losses, whereas melanomas show multiple segmental CNAs, including partial chromosomal gains and deletions (Bastian et al. 2002; North et al. 2013; Yélamos et al. 2015). Comparative genomic hybridization (CGH) is widely regarded as the reference standard for CNA analysis in this setting because it reliably discriminates between simple numerical aberrations and the complex segmental patterns typical of malignancy (Bastian et al. 2002; North et al. 2013; Yélamos et al. 2015). However, array-CGH is technically demanding and limited to specialized laboratories.

Alternative CNA detection approaches have become increasingly available. Shallow whole-genome sequencing (sWGS) provides genome-wide CNA profiles at low sequencing depth and is suitable for FFPE tissue, with diagnostic sensitivity comparable to CGH in melanocytic tumors (Alomari et al. 2020; Geiersbach et al. 2022). CNA profiles can also be derived from methylation sequencing data based on sequencing coverage signals, enabling copy-number analysis from the same data used for methylation-based tumor classification (Tran et al. 2025).

Despite their growing use, no prior study has systematically compared sWGS- and methylation-derived CNA profiles with CGH specifically in proliferative nodules and melanomas arising within congenital nevi. Here, we compare CNA detection across all three platforms and assess these findings in the context of available clinical follow-up.

2 | Methods

2.1 | Study Cohort

Children and young adults (0–30 years) with atypical melanocytic proliferations arising within a congenital melanocytic nevus between 2005 and 2024 were included. Cases originated either from referral specimens evaluated for expert dermatopathological consultation or from patients treated at the University Hospital Tübingen. Archival FFPE samples were re-evaluated, and 14 of 28 eligible cases were included after excluding samples with insufficient material or DNA yield. Sixteen lesions from these 14 patients were analyzed, as one patient had three nodules excised at different time points. Written informed consent was obtained where applicable; archival cases older than 5 years were included under an institutional consent waiver.

2.2 | Histology and Molecular Classification

Only lesions in which morphology alone did not allow reliable distinction between PN and melanoma were included. All cases were jointly assessed by at least two dermatopathologists specialized in melanocytic tumors. Molecular classification followed the criteria of Bastian et al. (2002). Lesions without CNAs or with whole-chromosome gains/losses and a single non–melanoma-typical arm-level aberration were classified as benign. Single melanoma-typical segmental aberrations were considered borderline. Multiple (≥ 2) segmental or arm-level aberrations defined malignant molecular profiles.

2.3 | Array Comparative Genomic Hybridization

Comparative genomic hybridization (CGH) analyses were performed in two distinct settings. For cases 1–7a and 7b, CGH was newly conducted retrospectively. DNA was extracted from formalin-fixed, paraffin-embedded (FFPE) tissue

samples, which were processed following standardized protocols for microdissection and DNA isolation. Microarray analyses were carried out using the SurePrint G3 Human CGH Microarray Kit 4×180K (Agilent Technologies, Santa Clara, USA). Hybridizations were scanned on an Agilent SureScan DX Microarray Scanner, with human reference DNA (female or male, Agilent Technologies) serving as the comparative reference. Data analysis was performed using Agilent Cytogenomics software (v5.1.2.1).

For cases 7c–14, existing CGH data from routine diagnostics, generated between 2009 and 2021, were utilized. Tumor tissue was manually microdissected from four to six 25-µm-thick paraffin sections, deparaffinized, and digested with proteinase K. DNA extraction and labeling were performed using genomic DNA universal linkage system labeling kits (Agilent Technologies, Santa Clara, USA). Hybridization employed the Agilent Human Genome CGH 105K microarray (Agilent Technologies). Arrays were scanned using an Agilent DNA microarray scanner, and image data were analyzed with Feature Extraction software (v10.5.1.1), DNA Analytics (v4.0.85), and Genomic Workbench Lite Edition (v6.5.0.18).

2.4 | sWGS

DNA was extracted from formalin-fixed, paraffin-embedded (FFPE) tissue samples, which were processed following standardized protocols for microdissection and DNA isolation. The DNA was quantified using the Qubit Fluorometer and dsDNA High sensitivity assay (both Thermo Fisher Scientific, Waltham, USA). The genomic fragment lengths of the samples were assessed with the Tapestation 4200 and the Genomic DNA ScreenTape Analysis (Agilent Technologies, Santa Clara, USA). Since some of the DNA samples showed discolorations, all of them were cleaned up with paramagnetic beads (SPRISelect, Beckman Coulter, Brea, USA) to reduce potential contaminants. 100 ng of the DNA was subsequently sheared and prepared for Next Generation Sequencing (NGS) using the NEBNext UltraShear FFPE DNA Library Prep Kit with NEBNext Unique Dual Index UMI Adaptors (both New England Biolabs, Ipswich, USA) with slight adjustments to the fragmentation incubation and the PCR protocol to accommodate for differences in the original sample qualities. The concentrations of the libraries were assessed using the Qubit Fluorometer and dsDNA High Sensitivity Assay-Kit (both Thermo Fisher Scientific, Waltham, USA), while fragment sizes were determined with the Fragment Analyzer 5300 and the Fragment Analyzer DNA HS NGS fragment Fragment kit (Agilent Technologies, Santa Clara, USA).

Sequencing was performed on a NovaSeq 6000 (Illumina, San Diego, CA, USA) in paired-end mode (2×154 bp) with an average of 177 million reads per sample.

2.5 | Methylation

DNA was extracted from formalin-fixed, paraffin-embedded (FFPE) tissue samples, which were processed following standardized protocols for microdissection and DNA isolation. The DNA was quantified using the Qubit Fluorometer and dsDNA High sensitivity assay (both Thermo Fisher Scientific, Waltham, USA). The genomic fragment lengths of the samples were assessed with the Tapestation 4200 and the Genomic DNA ScreenTape (both Agilent Technologies, Santa Clara, USA).

200 ng of DNA were prepared using the Twist Targeted Methylation Sequencing Workflow (Twist Bioscience, South San Francisco, USA) including the NEBNext Enzymatic Methyl-seq Library Preparation Protocol (New England Biolabs, Ipswich, USA) according to the manufacturers' protocol with 8-plex pre-capture pooling and targeted enrichment using the Twist Human Methylome enrichment panel. The concentrations of the libraries and pools were assessed using the Qubit Fluorometer and dsDNA High Sensitivity Assay-Kit (both Thermo Fisher Scientific, Waltham, USA), while fragment sizes were determined with the TapeStation 4200 and the High Sensitivity D1000 ScreenTape (both Agilent Technologies, Santa Clara, USA).

Sequencing was performed on a NovaSeq 6000 (Illumina, San Diego, CA, USA) in paired-end mode (2×154 bp) with an average of 227 million reads per sample.

CNA profiles derived from methylation sequencing data were generated from coverage-based signals, analogous to sequencing-based approaches, and therefore differ in resolution and sensitivity from array-based CGH.

For cases 1–7b, all analyses (aCGH, sWGS, and methylation sequencing) were performed using DNA extracted from the same FFPE tissue block. For cases 7c–14, analyses were conducted either on previously extracted stored DNA or on newly extracted DNA from the same FFPE block that had been used for aCGH.

2.6 | Sequencing

Shallow whole-genome sequencing (sWGS) and methylation sequencing (EM-seq) data as well as quality control were analyzed with an in-house pipeline called megSAP (version archived at Zenodo: https://zenodo.org/records/15063428). Sequencing reads were mapped to human genome reference GRCh38 using BWA-MEM2 for sWGS and Bismark for EM-seq (Krueger and Andrews 2011; Vasimuddin et al. 2019).

Mean coverage was 6.78× (range: 5.57–7.62) and 78.01× (range: 19.48–137.31) for sWGS and EM-seq respectively.

2.7 | Copy-Number Analysis

Copy-number alteration (CNA) analysis from sWGS and EM-seq data was performed using ClinCNV, a segmentation-based algorithm optimized for low-coverage whole-genome and targeted sequencing data (Demidov and Ossowski 2019). As no matched normal samples were available, CNA calling was performed using a tumor-only approach, assuming diploidy across the majority of the genome.

Coverage tracks were generated at 10 kb resolution, and GC correction was applied. CNA detection was executed with tumor-only mode using the following parameters:

--onlyTumor, --scoreS 1000, --lengthS 10, --minimumNumOfElemsInCluster 15, --purityStep 5, --clonePenalty 1000, --minimumPurity 5, --filterStep 0, with hg38 as the reference genome. Pseudoautosomal regions on chromosome X were excluded from the analysis to avoid sex-related copy number bias.

All detected CNA profiles were assessed by manual inspection. CNAs were categorized as whole chromosome or chromosome arm gains and deletions.

2.8 | Statistics

Statistical analyses were performed using Microsoft Excel (version 16.0). Descriptive statistics were calculated as appropriate. Concordance between CNA profiles obtained by aCGH, sWGS, and methylation sequencing was quantified using the Jaccard similarity coefficient, defined as the ratio of shared to total aberrations for each method pair. Heatmap visualizations were generated using Morpheus (Broad Institute; https://software.broadinstitute.org/morpheus/).

2.9 | Use of Artificial Intelligence Tools

ChatGPT (OpenAI) was used for limited language editing and text formulation. All scientific content and interpretations were developed and verified by the authors.

3 | Results

3.1 | Epidemiology, Clinical and Histological Presentation

The cohort included 14 patients aged 8 days to 26 years (nine males, five females). Most lesions arose within giant CMN located on the back or trunk (Figure 1a–c). Two cases involved congenital blue nevi, and two involved medium- or small-sized CMN with atypical features. Histopathologically, most nodules represented proliferative nodules (PN), including spitzoid variants requiring molecular workup for classification (Figure 1d,e). Follow-up ranged from 2 to 94 months. Three patients died from

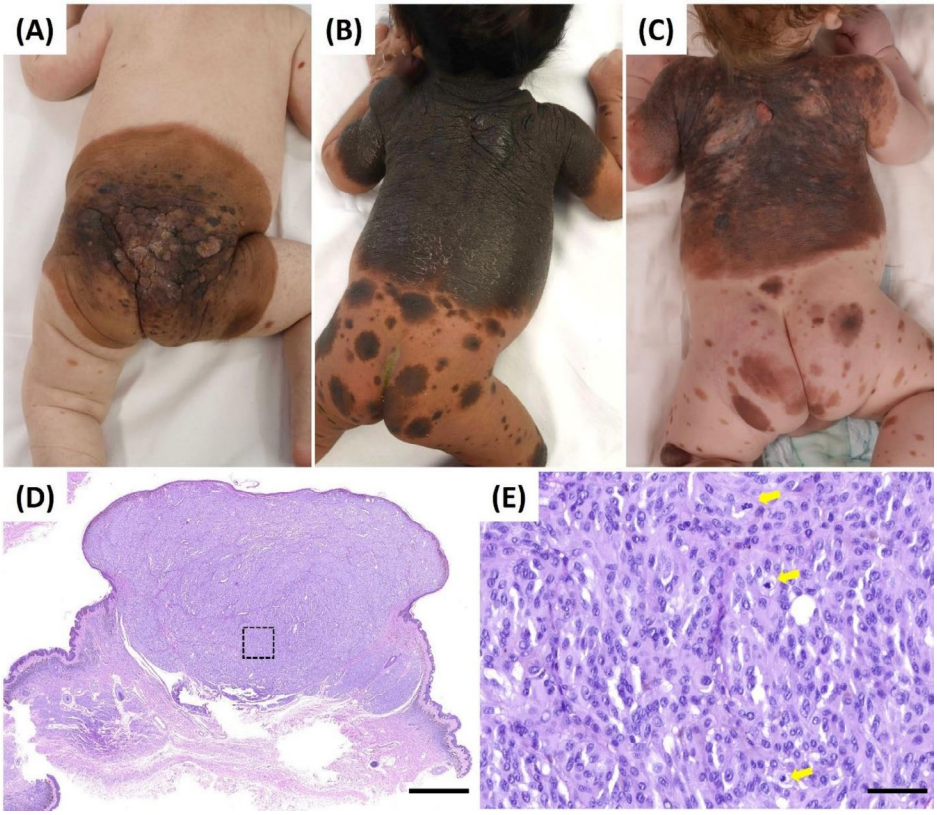

FIGURE 1 | Clinical presentation and histopathology of proliferative nodules in congenital melanocytic nevi. (A–C) Clinical photographs of three patients (A: Case 6; B: Case 8; C: Case 10) with giant congenital melanocytic nevi on the back, each demonstrating extensive pigmentation, satellite lesions, and multiple nodular proliferations raising concern for atypical melanocytic growth. (D, E) Histopathology of case 8 (hematoxylin and eosin). (D) Low-power view of a proliferative nodule arising within a congenital nevus. The lesion shows expansile growth within the dermis, with residual congenital nevus components visible at the periphery (scale bar: 2 mm). (E) High-power magnification of the area shown in (D), demonstrating pleomorphic epithelioid melanocytic cells with enlarged nuclei, prominent nucleoli, and several mitotic figures, three of which are highlighted by yellow arrows (scale bar: 50 μm).

TABLE 1 | Clinical and histopathological characteristics of the study cohort.

Case	Age	Sex	Clinical	Histology	Follow-up
1	15 years	M	Nodule in CMN, head/neck	PN on CMN	82 months, D
2	5 years	M	CMN, scalp	PN on CMN	14 months, D
3	3 years	F	Nodule in CMN, right hip	PN on CMN	17 months, A
4	4 years	F	Dark pigmented nodule in CMN, right shoulder	PN on CMN	48 months, A
5	15 years	M	Medium-sized CN with nodular areas on the back of the left hand	Atypical spitzoid PN on CMN	87 months, A
6	2 months	F	CMN with multiple nodular areas, buttock	PN on CMN	49 months, A
7a	5 months	F	CMN with multiple nodular areas, back	PN on CMN	2 months, D (after excision of the lymph node metastasis)
7b	11 months		CMN with multiple nodular areas, back	PN on CMN	
7c	2 years		Nodular swelling, left axilla	lymph node metastasis	
8	1 years	F	CMN with multiple nodular areas, back	PN on CMN	36 months, A
9	8 days	F	CMN with darker areas, right shoulder	PN on CMN	26 months, A
10	3 months	M	CMN with nodular areas, back	PN on CMN	n.a.
11	10 years	F	n.a.	PN on congenital blue nevus	n.a.
12	17 years	M	n.a.	PN on CMN	94 months, A
13	7 years	M	n.a.	PN on large congenital blue nevus	n.a.
14	26 years	M	Small, papillomatous CMN	Spitzoid PN on CMN	n.a.

Abbreviations: A, alive without disease; CMN, congenital melanocytic nevus (giant unless otherwise specified); D, deceased; n.a., not available; PN, proliferative nodule.

their disease, seven remained disease-free, and four lacked follow-up (Table 1).

3.2 | Comparative Analysis of Copy Number Alteration Detection by aCGH, sWGS, and Methylation Sequencing

All lesions were analyzed by aCGH, sWGS, and methylation sequencing, and all detected aberrations are listed in Table 2. Across the cohort, the platforms revealed a broadly consistent pattern of chromosomal gains and losses, but with marked differences in the number and resolution of detected events. aCGH identified 39 CNAs, whereas sWGS and methylation sequencing detected 60 and 66, respectively. Despite this, substantial overlap existed: 34 CNAs were shared between aCGH and sWGS, 34 between aCGH and methylation, and 45 between sWGS and methylation. A core set of 32 CNAs was concordantly detected across all three methods.

As expected, aCGH predominantly captured broad whole-chromosome alterations, while sWGS and methylation sequencing revealed numerous additional subchromosomal segmental and focal events. Methylation sequencing, in particular, identified recurrent terminal and arm-level deletions (e.g., del(20q11.21–qter), del(8q)) that were not detected by either aCGH or sWGS, suggesting increased sensitivity to focal or possibly subclonal aberrations. Jaccard similarity coefficients demonstrated the highest concordance between sWGS and methylation sequencing (mean 0.67), followed by aCGH versus sWGS (0.64) and aCGH versus methylation (0.49). Cases with extensive aneuploidy—such as cases 3, 4, 7c, 8, 10, and 12—showed perfect concordance across all methods, whereas cases with few aberrations exhibited greater variability, largely driven by additional focal events detected by methylation sequencing.

To visualize CNA burden across the cohort, a heatmap summarizing the number of CNAs per case and platform was generated, together with representative CNA profiles illustrating platform-specific resolution differences (Figure 2). In addition, representative genome-wide CNA profiles illustrating platform-specific resolution differences and concordance patterns are shown in Figure S1. Beyond the raw CNA counts,

TABLE 2 | Copy number alterations detected by aCGH, sWGS, and methylation sequencing across all cases.

Case	CGH	sWGS	Methylation
1	del(5, 7, 10, 12)	del(5, 7, 10, 12)	del(5p, 7, 10q, 12q)
2	gain(1q, 13q12.2–q32.1); del(3, 5p10–p12, 5q12.1–q14.1, 9, 10, 11, 12, 14, 17, 21)	gain(1, 2, 4, 6p, 7q, 13q12.12–q21.32, 13q22.1–q32.1, 15, 22); del(3, 5p10–p12, 5q12.1–q35.1, 9, 10, 11, 12, 14, 17, 21)	gain(1, 2, 4, 6p, 7, 13q12.12–q21.32, 13q22.1–q32.1, 15, 22); del(3p, 5q12.1–q14.1, 9, 10, 11p, 12, 14, 17, 21)
3	gain(2, 8, 13, 20, 22)	gain(2, 8, 13, 20, 22)	gain(2, 8, 13, 20, 22)
4	gain(6, 8, 9, 16, 18, 19, 20)	gain(6, 8, 9, 16, 18, 19, 20)	gain(6, 8, 9, 16, 18, 19, 20)
5	del(4q22.2–q28.2, 9)	gain(1p22.2–p36.13, 3p12.3–p25.3, 3q11.2–qter, 5p12–p13.3, 5q, 8q12.1–q24.23, 11q, 12q12–q23.3, 15q12–q25.2); del(1p36.13–pter, 2, 4q22.2–q28.2, 6q12–q22.31, 9, 16p)	gain(3p12.3–p25.3, 3q11.2–qter, 5p12–p15.3, 5q, 11p11.2–p15.4, 11q, 12q12–q23.3); del(1p36.13–pter, 4q22.2–q28.2, 9, 16)
6	gain(4, 8, 9, 12, 13, 14, 16, 19, 20, 21, 22); del(5, 10, 18)	gain(4, 8, 9, 12, 13, 14, 16q11.2–q24.1, 21); del(5, 10, 18)	gain(4, 9, 12, 13, 14, 16q11.2–q24.1, 19q13.31–q13.33, 21); del(1p32.2–pter, 5, 6p12.2–p22.2, 10, 18)
7a	gain(7, 8, 9, 12, 13, 16q, 17, 19, 20, 22); del(5, 10)	gain(7, 8, 9, 12, 13, 16q, 17q, 22); del(5, 10)	gain(7, 8, 9, 12, 13, 16p11.2–pter, 16q12.2–qter, 17, 19p13.11–pter, 19q13.11–q13.33, 22); del(5, 10)
7b	del(7)	gain(5q11.1–q33.1); del(7, 8q11.1–q23.3, 16p12.1–p13.3)	del(7)
7c	gain(1q, 7, 8, 20); del(3q13.3–qter, 5, 11, 16q, 17, 18)	gain(1q, 7, 8, 20); del(3q12.2–qter, 5, 11, 16q, 17, 18)	gain(1q, 7, 8, 20); del(3q12.2–qter, 5, 11, 16q, 17, 18)
8	gain(1q, 8, 16, 20); del(3, 5, 7, 11, 12, 14, 19, 21)	gain(1q, 8, 16, 20); del(3, 5, 7, 11, 12, 14, 19, 21)	gain(1q, 8, 16, 20); del(3, 5, 7, 11, 12, 14, 19, 21)
9	none	none	del(20q11.21–qter)
10	gain(7, 8, 12, 13, 16, 18, 20, 21); del(3)	gain(7, 8, 12, 13, 16, 18, 20, 21); del(3)	gain(7, 8, 12, 13, 16, 18, 20, 21); del(3)
11	none	none	del(8q)
12	gain(5, 15, 18, 20, 21, 22)	gain(5, 15, 18, 20, 21, 22)	gain(5, 15, 18, 20, 21, 22)
13	gain(6p21.1–pter)	gain(6p22.2–pter)	gain(6p22.2–pter); del(8q11.1–q24.23, 13q12.13–q33.3)
14	none	none	del(20q11.21–qter)

Note: For each lesion, all chromosomal gains and losses identified by array comparative genomic hybridization (aCGH), shallow whole-genome sequencing (sWGS), and methylation-derived CNA analysis are listed. Chromosomal alterations are reported using a standardized nomenclature. Whole-chromosome events are indicated by chromosome number (e.g., 5), chromosome-arm alterations by p or q designation (e.g., 1q), and segmental alterations by genomic coordinates (e.g., 13q12.2–q32.1). Abbreviations: del, deletion; gain, copy number gain; none, no detectable CNAs; pter, terminal end of the short arm; qter, terminal end of the long arm.

we assessed how platform-specific variation influenced molecular classification (Table 3). Based on established CGH-derived criteria, where lesions with no CNAs or exclusively whole-chromosome gains or losses are considered benign, and profiles with two or more segmental or arm-level aberrations are classified as malignant, aCGH classified most lesions as benign (13/16), whereas sWGS and methylation sequencing resulted in malignant classifications in 5/16 and 7/16 cases, respectively. Six cases showed complete concordance across all platforms, four showed minor discrepancies, and six displayed major discrepancies that shifted the diagnostic category. Minor discrepancies were defined as differences in the number or type of detected CNAs that did not alter the resulting molecular classification, whereas major discrepancies were defined as discordances that shifted the diagnostic category (benign, borderline, or malignant). Concordance of molecular classification (benign, borderline, malignant) across platforms is summarized in Table S1, highlighting discordant classifications in 6 of 16 cases. These divergences were primarily driven by additional segmental or focal CNAs detected by sWGS or

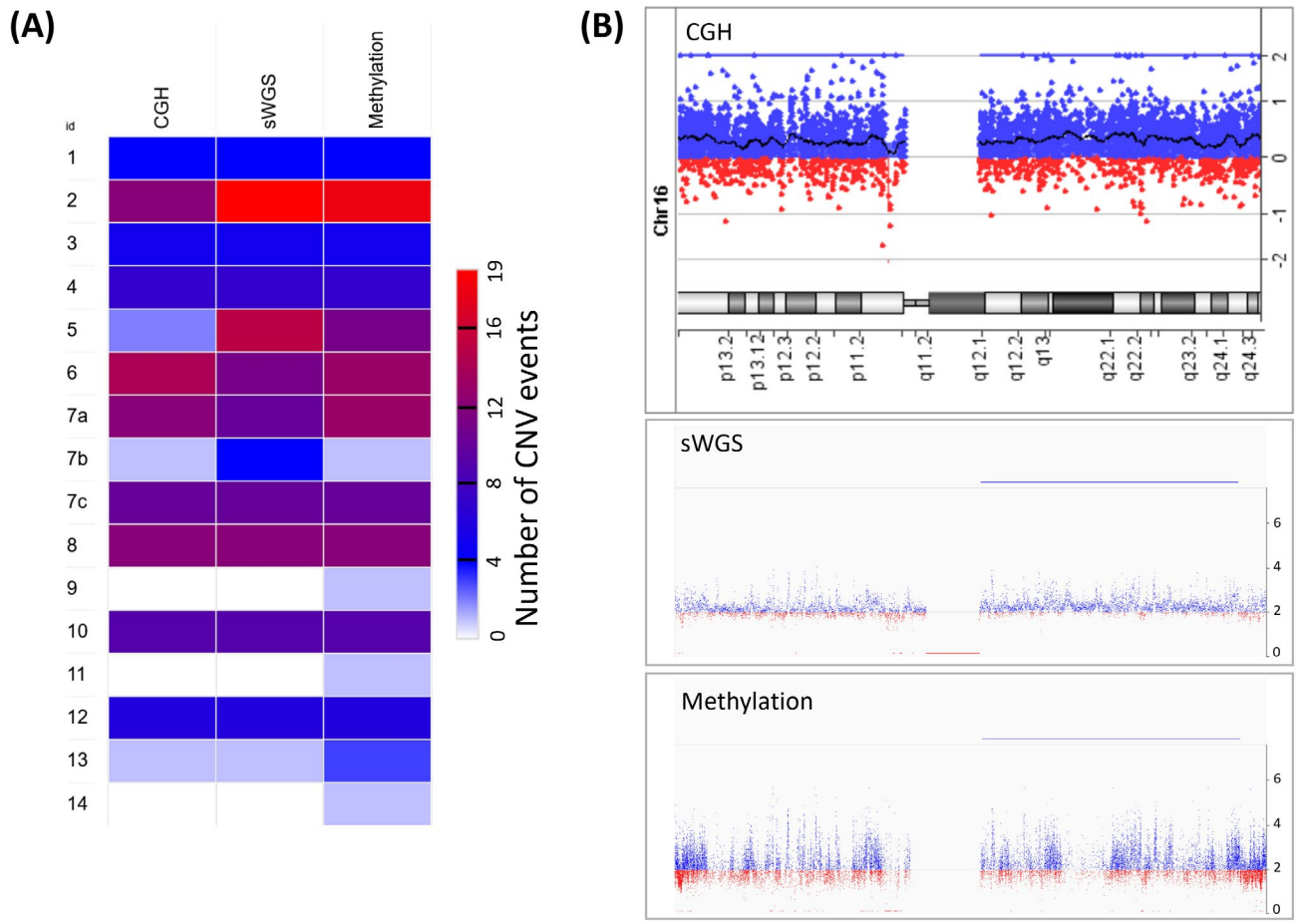

FIGURE 2 | Cross-platform comparison of CNV detection by aCGH, sWGS, and methylation sequencing. (A) Heatmap showing the number of chromosomal, arm-level, and segmental CNVs detected per case across all three platforms. High-burden cases demonstrate strong cross-platform concordance, whereas low-burden lesions display additional focal alterations, predominantly detected by methylation sequencing. (B) Exemplary CNA profiles of chromosome 16 from case 6. While aCGH identifies a whole-chromosome gain, both sWGS and methylation sequencing detect only a long segmental gain on 16q and do not call the gain on 16p, illustrating platform-specific differences in resolution and segmentation. CGH data are displayed on a $\log_2$ ratio scale, whereas for sWGS and methylation sequencing the y-axis represents estimated absolute copy number on a linear scale, with 2 corresponding to diploidy.

methylation sequencing, underscoring the challenge of applying CGH-based criteria to higher-resolution platforms.

3.3 | Correlation of Clinical Outcome

Clinical follow-up was reviewed to assess the relationship between molecular classifications and patient outcomes. Interpretation was limited in patients with giant congenital nevi containing multiple proliferative nodules, as the excised lesion might not represent the biologically relevant precursor of metastasis. Therefore, clinical outcome data were interpreted descriptively, and no formal statistical correlation analysis was performed.

This issue was most evident in patient 7, from whom three distinct nodules were sampled over time (cases 7a, 7b, and 7c). Cases 7a and 7b showed differing CNA patterns across platforms but were classified as benign by aCGH (and by methylation for 7b). In contrast, case 7c represented the lymph node metastasis and exhibited a highly complex CNA profile characteristic of melanoma. Neither 7a nor 7b shared the CNA pattern of the metastatic lesion, suggesting that the true primary melanoma node was not sampled. Thus, the molecular classifications of 7a and 7b cannot be directly correlated with the patient's adverse clinical course; these findings suggest they represent independent events.

Other discordant cases showed similar diagnostic uncertainty. In case 1, aCGH and sWGS classified the lesion as benign, whereas methylation sequencing detected arm-level deletions consistent with a malignant profile. The patient ultimately died; however, due to the multifocal nature of the congenital nevus, it remains unclear whether the analyzed nodule represented the lesion that gave rise to metastasis. In contrast, cases 5 and 6 showed benign CNA profiles by aCGH but malignant-appearing profiles by sWGS and methylation analysis; both patients remained disease-free. Case 13 showed borderline results by aCGH and sWGS but a malignant CNA profile derived from methylation sequencing; no clinical follow-up was available.

Across the cohort, three patients experienced fatal outcomes. Because several of these patients had multiple nodules and the true primary melanoma focus often could not be unequivocally

TABLE 3 | Molecular classifications based on CNA patterns detected by aCGH, sWGS, and methylation sequencing.

Case	CGH	sWGS	Methylation	Discrepancy
1	4 chr – **B**	4 chr – **B**	1 chr, 3 arm – **M**	Major
2	8 chr, 1 arm, 3 seg – **M**	13 chr, 2 arm, 4 seg – **M**	12 chr, 3 arm, 3 seg – **M**	Minor
3	5 chr – **B**	5 chr – **B**	5 chr – **B**	No
4	7 chr – **B**	7 chr – **B**	7 chr – **B**	No
5	1 chr, 1 seg – **B**	1 chr, 3 arm, 9 seg – **B**	2 chr, 2 arm, 7 seg – **M**	Major
6	14 chr – **B**	10 chr, 1 seg – **B**	9 chr, 4 seg – **M**	Major
7a	11 chr, 1 arm – **B**	8 chr, 2 arm – **M**	8 chr, 4 seg – **M**	Major
7b	1 chr – **B**	1 chr, 3 seg – **M**	1 chr – **B**	Major
7c	7 chr, 2 arm, 1 seg – **M**	7 chr, 2 arm, 1 seg – **M**	7 chr, 2 arm, 1 seg – **M**	No
8	11 chr, 1 arm – **B**	11 chr, 1 arm – **B**	11 chr, 1 arm – **B**	No
9	none – **B**	none – **B**	1 seg – **B**	Minor
10	9 chr – **B**	9 chr – **B**	9 chr – **B**	No
11	none – **B**	none – **B**	1 arm – **B**	Minor
12	6 chr – **B**	6 chr – **B**	6 chr – **B**	No
13	1 seg – **BL**	1 seg – **BL**	3 seg – **M**	Major
14	none – **B**	none – **B**	1 seg – **B**	Minor

Note: Shown are the numbers of whole-chromosome (chr), chromosome-arm (arm), and segmental (seg) alterations per platform, the resulting molecular classification (B = benign, BL = borderline, M = malignant), and the degree of discrepancy between methods.
Abbreviations: aCGH, array comparative genomic hybridization; arm, chromosome arm; B, benign; BL, borderline; chr, chromosome; M, malignant; seg, segment; sWGS, shallow whole-genome sequencing.

identified, formal performance metrics such as sensitivity and specificity could not be reliably established at the lesion level. Qualitatively, aCGH tended to classify fewer lesions as malignant than sWGS and methylation sequencing, particularly in patients with an overall benign clinical course, whereas the higher-resolution platforms more often yielded malignant CNA patterns, including in lesions from patients who remained disease-free. These observations highlight both the increased sensitivity of sWGS and methylation-based CNA analysis and the difficulty of attributing biological significance to small focal aberrations in multifocal congenital nevi where the causative melanoma precursor may remain unsampled.

4 | Discussion

Although aCGH, sWGS, and methylation-sequencing-based CNA analysis have often been described as comparable approaches for the detection of larger CNAs, our study demonstrates that relevant differences emerge when these methods are applied to atypical melanocytic proliferations in congenital nevi. Previous studies have reported high concordance between aCGH and next-generation sequencing (NGS)–based approaches for detecting broad CNAs in well-characterized genomic regions (Coutelier et al. 2022; Hayes et al. 2013; Scheinin et al. 2014; Wang, Lan, et al. 2025; Wang, Tao, et al. 2025). In contrast, we observed substantial variability in the detection of segmental and focal aberrations, which in several cases resulted in divergent molecular classifications. CNA inference from targeted methylation sequencing is based on sequencing-derived coverage signals and is therefore technically more comparable to sequencing-based approaches such as sWGS than to array-based CGH. This may partly explain the higher concordance observed between sWGS and methylation-derived CNA profiles in our cohort. At the same time, the increased sensitivity of sequencing-based approaches may lead to the detection of smaller or subclonal alterations that are not captured by CGH. These discrepancies likely reflect differences in technical resolution, genomic coverage, and analytical sensitivity across platforms, and may represent either biologically relevant alterations or technical effects such as increased sensitivity, over-segmentation, or detection of low-level subclonal events (Coutelier et al. 2022; Hayes et al. 2013; Scheinin et al. 2014; Wang, Lan, et al. 2025; Wang, Tao, et al. 2025).

Interpreting molecular findings in this clinical setting is inherently challenging, particularly in patients with giant congenital nevi who frequently harbor multiple proliferative nodules. In such cases, it is often unclear whether the sampled lesion corresponds to the biologically relevant precursor of metastasis. This issue has been repeatedly emphasized in the literature (Vergier et al. 2016; Yélamos et al. 2015) and was illustrated most clearly in our cohort by patient 7. This aligns with prior reports noting that melanomas arising in congenital nevi often develop within complex, heterogeneous nodular fields where histology and molecular profiles may diverge (Bastian et al. 2002; Merkel et al. 2019; Vergier et al. 2016; Yélamos et al. 2015).

Methylation array–based approaches have increasingly been applied in melanocytic lesions for tumor classification and CNA

inference, with recent studies demonstrating their diagnostic potential (Miele et al. 2025; Rossi et al. 2026). In contrast, the present study employs a targeted methylation sequencing approach, in which CNA inference is derived from sequencing-based coverage signals. This methodological difference is important, as sequencing-based approaches may differ from array-based methods in genomic coverage, resolution, and noise characteristics. In this context, it is important to emphasize that current diagnostic criteria for molecular classification in congenital nevi and proliferative nodules were developed using CGH (Alomari et al. 2020; Bastian et al. 2002; North et al. 2013; Vergier et al. 2016). Numerical aberrations involving whole chromosomes are considered typical for benign proliferative nodules, while melanomas are characterized by multiple segmental aberrations (Bastian et al. 2002; Merkel et al. 2019; Vergier et al. 2016; Yélamos et al. 2015). Because these criteria were validated in cohorts assessed by CGH, they may not directly translate to higher-resolution platforms. sWGS and methylation sequencing exhibit increased sensitivity for detecting small CNAs or subclonal aberrations (< 100 kb), particularly in FFPE tissue (Ardakani et al. 2017; Bauer and Bastian 2006; Tran et al. 2025; Van der Linden et al. 2020). While these additional findings might capture biologically meaningful alterations, they might also represent low-level or focal changes without prognostic significance, raising the possibility of diagnostic overinterpretation (Ardakani et al. 2017; Bauer and Bastian 2006; Van der Linden et al. 2020). Importantly, our data do not allow definitive discrimination between these possibilities and therefore primarily demonstrate platform-dependent discordance rather than systematic overcalling of malignancy. Some of the additional alterations detected by higher-resolution approaches involve chromosomal regions implicated in melanoma biology, such as losses on chromosome 9p affecting the CDKN2A locus (Bastian et al. 2002; North et al. 2013). However, these alterations were not consistently observed and did not form recurrent patterns allowing reliable diagnostic interpretation.

Moreover, the additional CNAs did not systematically correspond to loci used in established melanoma diagnostic assays based on CGH (Bastian et al. 2002; North et al. 2013) and often represented small focal or terminal changes of uncertain significance.

In the other direction, in tissue sections selected for DNA extraction from ambiguous neoplasms, anomalous mosaic clones may be present at levels too low to meet detection thresholds, a limitation that has been described for both array-based and low-pass sequencing approaches (Liu et al. 2023; Robberecht et al. 2010).

Our findings therefore support the need for platform-adapted diagnostic frameworks. High-resolution platforms such as sWGS and methylation sequencing provide technical advantages—including improved genomic resolution and the ability to extract CNA data from the same sample used for methylation classification—but their increased sensitivity must be balanced against the risk of upstaging otherwise benign lesions. Larger, prospectively collected cohorts including unequivocally benign proliferative nodules and melanomas arising within congenital nevi with systematic outcome correlation will be essential to delineate which CNA patterns detected by higher-resolution methods carry true biological and prognostic relevance. Targeted validation with orthogonal techniques like digital PCR, FISH, or MLPA, or deeper coverage with targeted NGS will be necessary to establish thresholds of reliability.

This study has several important limitations. First, the cohort size is inherently small due to the rarity of proliferative nodules and melanomas arising in congenital nevi, which limits statistical power and precludes robust outcome-based analyses such as disease-free survival or progression. Second, many patients had multiple nodules, and in some cases—including patient 7—the exact melanoma precursor could not be identified, preventing definitive lesion-level outcome correlation. Therefore, clinical correlations are descriptive rather than inferential. In addition, ancillary markers such as PRAME immunohistochemistry and TERT promoter mutation analysis were not systematically available across the cohort and could therefore not be integrated into the present comparative analysis. Future prospective studies combining CNA profiling with additional molecular and immunohistochemical markers may help to further clarify the biological significance of discordant findings. Third, inherent differences between the platforms—including resolution, noise characteristics, and algorithmic approaches—likely contributed to discordances. Finally, the retrospective use of archival FFPE samples introduces variability in DNA quality and tumor content, which may influence CNA detection.

In summary, while all three platforms reliably captured broad chromosomal alterations, sWGS and methylation sequencing identified substantially more focal and segmental CNAs. These differences significantly influenced molecular classification and must be interpreted cautiously, particularly in the setting of multinodular congenital nevi where the melanoma precursor may remain unsampled. Until platform-specific diagnostic criteria are established and validated in larger outcome-linked cohorts, CGH currently represents the most historically validated approach for molecular risk stratification in proliferative nodules arising within congenital nevi.

Author Contributions

Dominik T. Schneider: writing – review and editing. **Anton Karelin:** data curation, writing – review and editing, investigation, validation, methodology, software, formal analysis. **Michaela Pogoda:** writing – review and editing, methodology, writing – original draft. **Heather C. Etchevers:** writing – review and editing, funding acquisition. **German Demidov:** writing – review and editing. **Daniel Aldea:** writing – review and editing. **Ines B. Brecht:** conceptualization, funding acquisition, writing – review and editing. **Susana Puig:** funding acquisition, writing – review and editing. **Michael Abele:** writing – review and editing. **Matthias Hahn:** data curation, investigation, writing – review and editing. **Stephan Forchhammer:** conceptualization, methodology, data curation, supervision, project administration, writing – review and editing, writing – original draft, funding acquisition, visualization, formal analysis, investigation. **Christopher Schroeder:** data curation, project administration, funding acquisition, writing – review and editing, methodology, validation, software, investigation, conceptualization, formal analysis, supervision.

Acknowledgments

The findings and conclusions in this report are those of the authors and do not necessarily represent the official position of the

European Commission. The study was funded by an EU Horizon Grant (Melanoma in Childhood, Adolescents, and Young Adults—MELCAYA, HORIZON-MISS-2021-CANCER-02, ref. 101096667). Open Access funding enabled and organized by Projekt DEAL.

Funding

This work was supported by the European Union through the Horizon Research and Innovation program under Grant Agreement No 101096667. NGS methods were performed with the support of the DFG-funded NGS Competence Center Tübingen (INST 37/1049–1), funded by the Deutsche Forschungsgemeinschaft (DFG, German Research Foundation) – Project-ID 286/2020B01—428994620. The STEP registry is funded by the Deutsche Kinderkrebsstiftung.

Ethics Statement

The study was approved by the Ethics Committee of the Medical Faculty of the University of Tübingen (Project ID 399/2023BO1) and conducted in accordance with the Declaration of Helsinki.

Consent

Written informed consent was given by all patients or their legal guardians. Consent was waived for deceased patients or samples older than 5 years.

Conflicts of Interest

A.K., I.B.B., M.P., G.D., M.A., D.T.S., D.A., H.C.E., and M.H.: None. S.P. received personal honoraria to her or contracts with her institution from Almirall, BMS, Cantabria, Eucerin, ISDIN, ISD, La Roche Posay, MSD, Novartis, Regeneron, Sunpharma. S.P.'s institution collaborates in research with Damae and Canfield. C.S. reports institutional grants from Illumina Inc. and Oxford Nanopore Technologies and research grants from BMS Stiftung Immunonkologie and Westdeutsche Studiengruppe GmbH outside the submitted work. S.F. received personal honoraria from Kyowa Kirin, Stemline, and Recordati Rare Diseases (speaker's honoraria, advisory board), as well as institutional grants from BioNTech SE, Neracare, and SkylineDX. All outside the submitted work.

Data Availability Statement

The data presented in this study are available on request from the corresponding author.

References

Alomari, A. K., J. R. Miedema, M. D. Carter, et al. 2020. "DNA Copy Number Changes Correlate With Clinical Behavior in Melanocytic Neoplasms: Proposal of an Algorithmic Approach." *Modern Pathology* 33, no. 7: 1307–1317.

Ardakani, N. M., C. Thomas, C. Robinson, et al. 2017. "Detection of Copy Number Variations in Melanocytic Lesions Utilising Array Based Comparative Genomic Hybridisation." *Pathology* 49, no. 3: 285–291.

Bastian, B. C., J. Xiong, I. J. Frieden, et al. 2002. "Genetic Changes in Neoplasms Arising in Congenital Melanocytic Nevi: Differences Between Nodular Proliferations and Melanomas." *American Journal of Pathology* 161, no. 4: 1163–1169.

Bauer, J., and B. C. Bastian. 2006. "Distinguishing Melanocytic Nevi From Melanoma by DNA Copy Number Changes: Comparative Genomic Hybridization as a Research and Diagnostic Tool." *Dermatologic Therapy* 19, no. 1: 40–49.

Coutelier, M., M. Holtgrewe, M. Jäger, et al. 2022. "Combining Callers Improves the Detection of Copy Number Variants From Whole-Genome Sequencing." *European Journal of Human Genetics* 30, no. 2: 178–186.

Demidov, G., and S. Ossowski. 2019. "ClinCNV: Novel Method for Allele-Specific Somatic Copy-Number Alterations Detection." *BioRxiv*, 837971.

Ferrari, A., I. B. Brecht, G. Gatta, et al. 2019. "Defining and Listing Very Rare Cancers of Paediatric Age: Consensus of the Joint Action on Rare Cancers in Cooperation With the European Cooperative Study Group for Pediatric Rare Tumors." *European Journal of Cancer* 110: 120–126.

Geiersbach, K. B., T. J. Gliem, S. M. Jenkins, et al. 2022. "Single-Nucleotide Polymorphism Array for Histologically Ambiguous Melanocytic Tumors." *Journal of Molecular Diagnostics* 24, no. 11: 1160–1170.

Hawryluk, E. B., D. Moustafa, D. Bartenstein, et al. 2020. "A Retrospective Multicenter Study of Fatal Pediatric Melanoma." *Journal of the American Academy of Dermatology* 83, no. 5: 1274–1281.

Hayes, J., A. Tzika, H. Thygesen, et al. 2013. "Diagnosis of Copy Number Variation by Illumina Next Generation Sequencing Is Comparable in Performance to Oligonucleotide Array Comparative Genomic Hybridisation." *Genomics* 102, no. 3: 174–181.

Krueger, F., and S. R. Andrews. 2011. "Bismark: A Flexible Aligner and Methylation Caller for Bisulfite-Seq Applications." *Bioinformatics* 27, no. 11: 1571–1572.

Liu, Y., S. Hao, X. Guo, et al. 2023. "Accuracy and Depth Evaluation of Clinical Low Pass Genome Sequencing in the Detection of Mosaic Aneuploidies and CNVs." *BMC Medical Genomics* 16, no. 1: 294.

McMullan, P., and J. M. Grant-Kels. 2025. "Childhood and Adolescent Melanoma: An Update." *Clinics in Dermatology* 43, no. 1: 16–23.

Merkel, E. A., L. S. Mohan, K. Shi, E. Panah, B. Zhang, and P. Gerami. 2019. "Paediatric Melanoma: Clinical Update, Genetic Basis, and Advances in Diagnosis." *Lancet Child & Adolescent Health* 3, no. 9: 646–654.

Miele, E., S. Rossi, A. Stracuzzi, et al. 2025. "Epigenomic Characterization and Therapeutic Challenges of Melanoma Arising in Giant Nevi in Pediatric Patients." *Discover Oncology* 16, no. 1: 2164.

North, J. P., S. S. Vemula, and B. C. Bastian. 2013. "Chromosomal Copy Number Analysis in Melanoma Diagnostics." In *Molecular Diagnostics for Melanoma: Methods and Protocols*, 199–226. Springer.

Pampena, R., V. Piccolo, M. Muscianese, et al. 2023. "Melanoma in Children: A Systematic Review and Individual Patient Meta-Analysis." *Journal of the European Academy of Dermatology and Venereology* 37: 1758–1776.

Pappo, A. S., V. McPherson, H. Pan, et al. 2021. "A Prospective, Comprehensive Registry That Integrates the Molecular Analysis of Pediatric and Adolescent Melanocytic Lesions." *Cancer* 127, no. 20: 3825–3831.

Pavlova, O., S. Fraitag, and D. Hohl. 2016. "5-Hydroxymethylcytosine Expression in Proliferative Nodules Arising Within Congenital Nevi Allows Differentiation From Malignant Melanoma." *Journal of Investigative Dermatology* 136, no. 12: 2453–2461.

Phadke, P. A., D. Rakheja, L. P. Le, et al. 2011. "Proliferative Nodules Arising Within Congenital Melanocytic Nevi: A Histologic, Immunohistochemical, and Molecular Analyses of 43 Cases." *American Journal of Surgical Pathology* 35, no. 5: 656–669.

Robberecht, C., J.-P. Fryns, and J. R. Vermeesch. 2010. "Piecing Together the Problems in Diagnosing Low-Level Chromosomal Mosaicism." *Genome Medicine* 2, no. 7: 47.

Rossi, S., S. Barresi, I. Giovannoni, et al. 2026. "Melanomas and Mesenchymal Tumors Arising in Giant Congenital Melanocytic Nevi: Clinico-Pathological and Molecular Characterization of a Case Series." *Pigment Cell & Melanoma Research* 39, no. 1: e70071.

Scheinin, I., D. Sie, H. Bengtsson, et al. 2014. "DNA Copy Number Analysis of Fresh and Formalin-Fixed Specimens by Shallow Whole-Genome Sequencing With Identification and Exclusion of Problematic Regions in the Genome Assembly." *Genome Research* 24, no. 12: 2022–2032.

Tran, Q. T., S. Jia, M. Z. Alom, et al. 2025. "Validation of Target-Enriched Enzymatic Methylation Sequencing for Brain Tumor Classification From Formalin-Fixed Paraffin Embedded-Derived DNA." *Brain Pathology* 35, no. 5: e70000.

Van der Linden, M., L. Raman, A. Vander Trappen, et al. 2020. "Detection of Copy Number Alterations by Shallow Whole-Genome Sequencing of Formalin-Fixed, Paraffin-Embedded Tumor Tissue." *Archives of Pathology & Laboratory Medicine* 144, no. 8: 974–981.

Vasimuddin, M., S. Misra, H. Li, and S. Aluru. 2019. "Efficient Architecture-Aware Acceleration of BWA-MEM for Multicore Systems." 2019 IEEE International Parallel and Distributed Processing Symposium (IPDPS).

Vergier, B., E. Laharanne, M. Prochazkova-Carlotti, et al. 2016. "Proliferative Nodules vs. Melanoma Arising in Giant Congenital Melanocytic Nevi During Childhood." *JAMA Dermatology* 152, no. 10: 1147–1151.

Wang, J., Y. Lan, H.-Y. Qi, et al. 2025. "Comparison of Fluorescence in Situ Hybridization, Next-Generation Sequencing, and DNA Methylation Microarray for Copy Number Variation Assessment in Gliomas." *Laboratory Investigation* 105, no. 7: 104168.

Wang, N., Z.-Y. Tao, T. Wu, et al. 2025. "Benchmarking Copy Number Variation Detection With Low-Coverage Whole-Genome Sequencing." *Briefings in Bioinformatics* 26, no. 5: bbaf514.

Yélamos, O., N. C. Arva, R. Obregon, et al. 2015. "A Comparative Study of Proliferative Nodules and Lethal Melanomas in Congenital Nevi From Children." *American Journal of Surgical Pathology* 39, no. 3: 405–415.

Yousif, R., C. Boull, P. Gerami, B. Nardone, K. L. Vivar, and W. Liszewski. 2021. "The Demographics and Trends in Pediatric Melanoma in the United States: An Analysis of the National Cancer Database." *Pediatric Dermatology* 38, no. 5: 1191–1197.

Supporting Information

Additional supporting information can be found online in the Supporting Information section. **Figure S1:** Representative genome-wide CNA profiles across platforms. Genome-wide copy number profiles of selected cases illustrating concordant (Case 12), discordant (Case 13), and low-burden (Case 14) CNA patterns across aCGH, sWGS, and methylation sequencing. While broad chromosomal alterations are consistently detected, higher-resolution sequencing-based approaches reveal additional focal events not captured by aCGH. aCGH profiles are shown as log2 ratios, whereas sWGS and methylation sequencing profiles represent estimated copy number (linear scale; diploid baseline = 2). Called CNAs are displayed below each profile, with gains indicated in blue and losses in red. **Table S1:** Molecular classification based on CNA profiles: B = benign; BL = borderline; M = malignant. Classification concordance indicates whether all three platforms yielded the same classification. **Data S1:** pcmr70097-sup-0002-Supinfo1.docx.